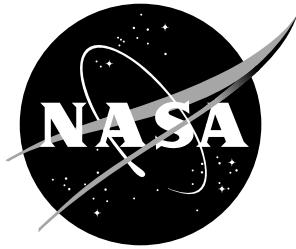


NASA/TM-2001-210861



The Linear Bicharacteristic Scheme for Electromagnetics

John H. Beggs
Langley Research Center, Hampton, Virginia

May 2001

The NASA STI Program Office ... in Profile

Since its founding, NASA has been dedicated to the advancement of aeronautics and space science. The NASA Scientific and Technical Information (STI) Program Office plays a key part in helping NASA maintain this important role.

The NASA STI Program Office is operated by Langley Research Center, the lead center for NASA's scientific and technical information. The NASA STI Program Office provides access to the NASA STI Database, the largest collection of aeronautical and space science STI in the world. The Program Office is also NASA's institutional mechanism for disseminating the results of its research and development activities. These results are published by NASA in the NASA STI Report Series, which includes the following report types:

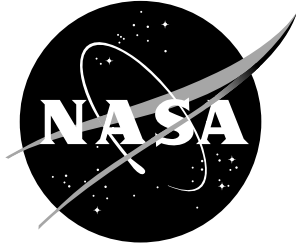
- **TECHNICAL PUBLICATION.** Reports of completed research or a major significant phase of research that present the results of NASA programs and include extensive data or theoretical analysis. Includes compilations of significant scientific and technical data and information deemed to be of continuing reference value. NASA counterpart of peer-reviewed formal professional papers, but having less stringent limitations on manuscript length and extent of graphic presentations.
- **TECHNICAL MEMORANDUM.** Scientific and technical findings that are preliminary or of specialized interest, e.g., quick release reports, working papers, and bibliographies that contain minimal annotation. Does not contain extensive analysis.
- **CONTRACTOR REPORT.** Scientific and technical findings by NASA-sponsored contractors and grantees.
- **CONFERENCE PUBLICATION.** Collected papers from scientific and technical conferences, symposia, seminars, or other meetings sponsored or co-sponsored by NASA.
- **SPECIAL PUBLICATION.** Scientific, technical, or historical information from NASA programs, projects, and missions, often concerned with subjects having substantial public interest.
- **TECHNICAL TRANSLATION.** English-language translations of foreign scientific and technical material pertinent to NASA's mission.

Specialized services that complement the STI Program Office's diverse offerings include creating custom thesauri, building customized databases, organizing and publishing research results... even providing videos.

For more information about the NASA STI Program Office, see the following:

- Access the NASA STI Program Home Page at ***<http://www.sti.nasa.gov>***
- E-mail your question via the Internet to help@sti.nasa.gov
- Fax your question to the NASA STI Help Desk at (301) 621-0134
- Phone the NASA STI Help Desk at (301) 621-0390
- Write to:
NASA STI Help Desk
NASA Center for AeroSpace Information
7121 Standard Drive
Hanover, MD 21076-1320

NASA/TM-2001-210861



The Linear Bicharacteristic Scheme for Electromagnetics

John H. Beggs
Langley Research Center, Hampton, Virginia

National Aeronautics and
Space Administration

Langley Research Center
Hampton, Virginia 23681-2199

May 2001

Available from:

NASA Center for AeroSpace Information (CASI)
7121 Standard Drive
Hanover, MD 21076-1320
(301) 621-0390

National Technical Information Service (NTIS)
5285 Port Royal Road
Springfield, VA 22161-2171
(703) 605-6000

Abstract

The upwind leapfrog or Linear Bicharacteristic Scheme (LBS) has previously been implemented and demonstrated on electromagnetic wave propagation problems. This report extends the Linear Bicharacteristic Scheme for computational electromagnetics to model lossy dielectric and magnetic materials and perfect electrical conductors. This is accomplished by proper implementation of the LBS for homogeneous lossy dielectric and magnetic media and for perfect electrical conductors. Heterogeneous media are modeled through implementation of surface boundary conditions and no special extrapolations or interpolations at dielectric material boundaries are required. Results are presented for one-dimensional model problems on both uniform and nonuniform grids, and the FDTD algorithm is chosen as a convenient reference algorithm for comparison. The results demonstrate that the explicit LBS is a dissipation-free, second-order accurate algorithm which uses a smaller stencil than the FDTD algorithm, yet it has approximately one-third the phase velocity error. The LBS is also more accurate on nonuniform grids.

1 Introduction

Numerical solutions of the Euler equations in Computational Fluid Dynamics (CFD) have illustrated the importance of treating a hyperbolic system of partial differential equations with the theory of characteristics and in an upwind manner (as opposed to symmetrically in space). These two features provide the motivation to use the Linear Bicharacteristic Scheme (LBS), or the upwind leapfrog method, for the construction of many practical wave propagation algorithms. In a hyperbolic system, the solutions (i.e. waves) propagate in preferred directions called characteristics. A characteristic can be defined as a propagation path along which a physical disturbance is propagated [1]. The relevance to Maxwell's equations is intuitively obvious because electromagnetic waves have preferred directions of propagation and finite propagation speeds.

The upwind leapfrog method has a more compact stencil compared with a classical leapfrog method. Clustering the stencil around the characteristic enables high accuracy to be achieved with a low operation count in a fully discrete way [2]. This leads to a more natural treatment of outer boundaries and material boundaries. The LBS treats the outer boundary condition naturally without nonreflecting approximations or matched layers. The interior point algorithm predicts the outgoing characteristic variables at the domain boundaries. Through knowledge of the wave propagation angle, the local coordinates can be rotated to align with the characteristics, at which the boundary condition becomes almost exact. Therefore, no extraneous boundary condition or matched layers are required, which can introduce errors into the solution. The LBS also offers a natural treatment of dielectric interfaces, without any extrapolation or interpolation of fields or material properties near material discontinuities.

The LBS was originally developed to improve unsteady solutions in computational acoustics and aeroacoustics [3]-[8]. It is a classical leapfrog algorithm, but is combined with upwind bias in the spatial derivatives. This approach preserves the time-reversibility of the leapfrog algorithm, which results in no dissipation, and it permits more flexibility by the ability to adopt a charac-

teristic based method. The use of characteristic variables allows the LBS to treat the outer computational boundaries naturally using the exact compatibility equations. The LBS offers a central storage approach with lower dispersion than the Yee algorithm, plus it generalizes much easier to nonuniform grids. It has previously been applied to two and three-dimensional free-space electromagnetic propagation and scattering problems [4], [7], [8].

The objective of this report is to extend the LBS to model both homogeneous and heterogeneous lossy dielectric and magnetic materials and perfect electrical conductors (PECs). Results are presented for several one-dimensional model problems, and the FDTD algorithm is chosen as a convenient reference for comparison. Sections 2 and 3 present the LBS implementation for homogeneous and heterogeneous materials, respectively. Section 4 discusses the outer radiation boundary condition and Section 5 reviews the Fourier analysis. Finally, Section 6 presents results for one-dimensional model problems and Section 7 provides concluding remarks.

2 Homogeneous Materials

Maxwell's equations for linear, homogeneous and lossy media in the one-dimensional TE case (taking $\partial/\partial y = \partial/\partial z = 0$) are

$$\frac{\partial E_y}{\partial t} = \frac{1}{\epsilon} \left(-\frac{\partial H_z}{\partial x} - \sigma E_y \right) \quad (1)$$

$$\frac{\partial H_z}{\partial t} = \frac{1}{\mu} \left(-\frac{\partial E_y}{\partial x} - \sigma^* H_z \right) \quad (2)$$

where σ and σ^* are the electric and magnetic conductivities, respectively. Using the electric displacement $D = \epsilon E$ and making the substitution $c = 1/\sqrt{\mu\epsilon}$ gives

$$\frac{\partial D_y}{\partial t} + \frac{\partial H_z}{\partial x} + \frac{\sigma}{\epsilon} D_y = 0 \quad (3)$$

$$\frac{1}{c^2} \frac{\partial H_z}{\partial t} + \frac{\partial D_y}{\partial x} + \frac{\sigma^*}{\mu c^2} H_z = 0 \quad (4)$$

The procedure for the LBS is to transform the dependent variables D_y and H_z to characteristic variables. Based upon the numerical method of characteristics for electromagnetics [9], information propagates (in one space dimension) along the characteristic curves specified by the characteristic equations

$$\frac{dx}{dt} = \pm c \quad (5)$$

which show that waves propagate in the $\pm x$ directions with a finite physical speed of c . The algorithm developed here is the simplest leapfrog scheme described by Iserles [10] combined with upwind bias, or simply, the Linear Bicharacteristic Scheme (LBS). To transform (3) and (4) into characteristic form, we first multiply (4) by c and then add and subtract from (3) to give

$$\frac{\partial \left(D_y + \frac{1}{c} H_z \right)}{\partial t} + c \frac{\partial \left(D_y + \frac{1}{c} H_z \right)}{\partial x} + \frac{\sigma}{\epsilon} D_y + \frac{\sigma^*}{\mu c} H_z = 0 \quad (6)$$

$$\frac{\partial \left(D_y - \frac{1}{c} H_z \right)}{\partial t} - c \frac{\partial \left(D_y - \frac{1}{c} H_z \right)}{\partial x} + \frac{\sigma}{\epsilon} D_y - \frac{\sigma^*}{\mu c} H_z = 0 \quad (7)$$

Now define

$$P = D_y + \frac{1}{c} H_z \quad (8)$$

$$Q = D_y - \frac{1}{c} H_z \quad (9)$$

to represent the right and left propagating solutions, respectively. P and Q are otherwise known as the characteristic variables. Using these definitions, (6) and (7) can be rewritten as

$$\frac{\partial P}{\partial t} + c \frac{\partial P}{\partial x} + \frac{1}{2} \left(\frac{\sigma}{\epsilon} + \frac{\sigma^*}{\mu} \right) P + \frac{1}{2} \left(\frac{\sigma}{\epsilon} - \frac{\sigma^*}{\mu} \right) Q = 0 \quad (10)$$

$$\frac{\partial Q}{\partial t} - c \frac{\partial Q}{\partial x} + \frac{1}{2} \left(\frac{\sigma}{\epsilon} - \frac{\sigma^*}{\mu} \right) P + \frac{1}{2} \left(\frac{\sigma}{\epsilon} + \frac{\sigma^*}{\mu} \right) Q = 0 \quad (11)$$

It is convenient to define and store the following coefficients before time-stepping begins

$$a = \frac{\sigma}{\epsilon} + \frac{\sigma^*}{\mu} \quad (12)$$

$$b = \frac{\sigma}{\epsilon} - \frac{\sigma^*}{\mu} \quad (13)$$

Equations (10) and (11) can be rewritten more simply as

$$\frac{\partial P}{\partial t} + c \frac{\partial P}{\partial x} + \frac{a}{2} P + \frac{b}{2} Q = 0 \quad (14)$$

$$\frac{\partial Q}{\partial t} - c \frac{\partial Q}{\partial x} + \frac{b}{2} P + \frac{a}{2} Q = 0 \quad (15)$$

To develop the discretized algorithm for a one-dimensional system, the stencils of Figure 1 are proposed for the LBS. To solve the wave propagation problem without introducing dissipation, it is necessary that the stencil have central symmetry so the scheme employed is reversible in time [2]. The stencil in Figure 1a is used for a right propagating wave and the stencil in Figure 1b is used for a left propagating wave. The upwind bias nature of these stencils is thus clearly evident. References [3], [2], [6], [7], [8] clearly show that the LBS is second-order accurate.

Note that the last two terms in (14) and (15) represent the electric and magnetic loss (or source) terms. A key element in developing an accurate LBS scheme is proper treatment of these source terms. Several methods for treating these source terms have already been investigated [6], [7], [8] for aeroacoustic applications. For electromagnetics, several methods for treating these source terms were investigated during this project. For example, one can index both source terms in (14) and (15) at time level n , which Thomas [6] has shown to be unstable. Another example would be to index both source terms at time level $n+1$ resulting in a semi-implicit method. Other examples involve applying an exponential transformation to (14) and (15) to eliminate the source term and then perform a linearization of the exponential terms in the discretized equations. However, the

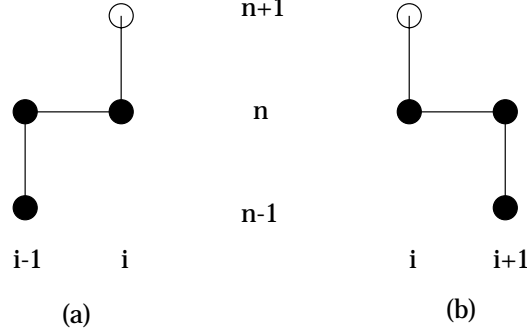


Figure 1: One-dimensional upwind leapfrog computational stencils for right-going (a) and left-going (b) characteristics.

method found to be most efficient and accurate is to index the self source term in (14) (i.e. P) at time level $n + 1$ and to index the coupled source term Q at time level n . This avoids a matrix solution at each grid point, and the formulation easily limits to the perfect conductor condition as $\sigma \rightarrow \infty$.

Using the stencils shown in Figure 1 and the source term indexing scheme outlined above, the resulting finite difference equations for (14) and (15) are

$$\frac{(P_i^{n+1} - P_i^n) + (P_{i-1}^n - P_{i-1}^{n-1})}{2\Delta t} + c \left(\frac{P_i^n - P_{i-1}^n}{\Delta x} \right) + \frac{a}{2} P_i^{n+1} + \frac{b}{2} Q_i^n = 0 \quad (16)$$

$$\frac{(Q_i^{n+1} - Q_i^n) + (Q_{i+1}^n - Q_{i+1}^{n-1})}{2\Delta t} - c \left(\frac{Q_{i+1}^n - Q_i^n}{\Delta x} \right) + \frac{a}{2} Q_i^{n+1} + \frac{b}{2} P_i^n = 0 \quad (17)$$

These equations can be rewritten in the form

$$(1 + a \Delta t) P_i^{n+1} = P_{i-1}^{n-1} + (1 - 2\nu) (P_i^n - P_{i-1}^n) - b \Delta t Q_i^n \quad (18)$$

$$(1 + a \Delta t) Q_i^{n+1} = Q_{i+1}^{n-1} - (1 - 2\nu) (Q_{i+1}^n - Q_i^n) - b \Delta t P_i^n \quad (19)$$

where $\nu = c\Delta t/\Delta x$ is the Courant number. We now rewrite equations (18) and (19) as

$$P_i^{n+1} = R_1^n / (1 + a \Delta t) \quad (20)$$

$$Q_i^{n+1} = R_2^n / (1 + a \Delta t) \quad (21)$$

where R_1^n and R_2^n are the residuals defined by

$$R_1^n = P_{i-1}^{n-1} + (1 - 2\nu) (P_i^n - P_{i-1}^n) - b \Delta t Q_i^n \quad (22)$$

$$R_2^n = Q_{i+1}^{n-1} - (1 - 2\nu) (Q_{i+1}^n - Q_i^n) - b \Delta t P_i^n \quad (23)$$

Equations (20) and (20) are the update equations for lossy dielectric and magnetic materials. Note that as $\sigma \rightarrow \infty$, then we have the PEC condition that $P_i^{n+1} = Q_i^{n+1} = 0$ as required.

3 Heterogeneous Dielectrics

One of the difficulties with the conventional FDTD algorithm is the error in treatment of material discontinuities. Recent research efforts have attempted to reduce this error source by suitable averaging of material properties across the interface or by interpolation or extrapolation of the electromagnetic fields near these material boundaries [11], [12]. The advantage of the LBS is that the characteristic based nature of the algorithm leads to a very natural treatment of dielectric interfaces. Since the LBS works with characteristic variables, the slope of characteristic curves in each material will be different, and the physical boundary conditions permit an elegant and efficient implementation of a dielectric interface boundary condition. This numerical boundary condition implements the physics exactly, with no averaging, interpolation or extrapolation required.

To implement the dielectric material interface boundary condition, consider the one-dimensional grid shown in Figure 2. The dielectric interface is located at grid point i and the dielectric materials

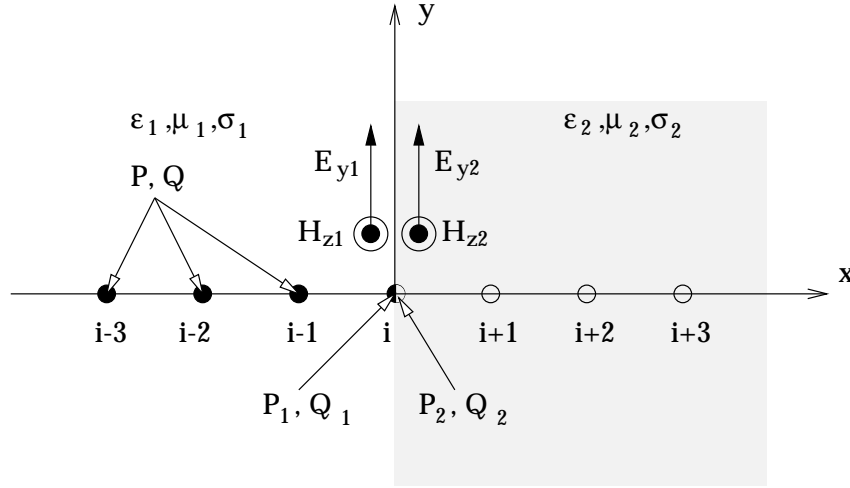


Figure 2: One-dimensional computational grid for the LBS showing characteristic variables, a dielectric interface located at cell i , and corresponding field components and characteristic variables used for the surface boundary condition.

can be lossy. The characteristic variables at grid point i , P_i and Q_i , are split into two components each: P_1, Q_1, P_2 and Q_2 . The terms P_1 and Q_1 exist just to the left of the material interface as shown in Figure 2. The remaining terms P_2 and Q_2 exist just to the right of the material interface. For material 1, equation (20) is used to predict the value for P_1^{n+1} at the boundary and for material 2, equation (21) is used to predict the value for Q_2^{n+1} . To complete the implementation, the Q_1^{n+1} and P_2^{n+1} terms must be updated. These terms are updated by enforcing the physical boundary conditions on the electromagnetic field at the material boundary. We can then solve for Q_1^{n+1} and P_2^{n+1} in terms of the “known” characteristic variables P_1^{n+1} and Q_2^{n+1} . To develop this procedure, the electromagnetic boundary conditions on the tangential field components are given by

$$E_{y1} = E_{y2} \Rightarrow \frac{D_{y1}}{\epsilon_1} = \frac{D_{y2}}{\epsilon_2} \quad (24)$$

$$H_{z1} = H_{z2} \quad (25)$$

For the right-going wave, substituting (24) and (25) into (8) gives

$$P_1^{n+1} = D_{y1}^{n+1} + \frac{1}{c_1} H_{z1}^{n+1} \quad (26)$$

$$= \frac{\epsilon_1}{2\epsilon_2} (P_2^{n+1} + Q_2^{n+1}) + \frac{c_2}{2c_1} (P_2^{n+1} - Q_2^{n+1}) \quad (27)$$

Similarly, substituting (24) and (25) into (9) yeilds

$$Q_2^{n+1} = D_{y2}^{n+1} - \frac{1}{c_2} H_{z2}^{n+1} \quad (28)$$

$$= \frac{\epsilon_2}{2\epsilon_1} (P_1^{n+1} + Q_1^{n+1}) - \frac{c_1}{2c_2} (P_1^{n+1} - Q_1^{n+1}) \quad (29)$$

Since P_1^{n+1} and Q_2^{n+1} are determined at boundary point i from the usual update equations (we treat them as “known” variables), it is necessary to express P_2^{n+1} and Q_1^{n+1} in terms of these variables. Rearranging (27) and (29) gives

$$P_2^{n+1} = T_1 P_1^{n+1} + \Gamma_1 Q_2^{n+1} \quad (30)$$

$$Q_1^{n+1} = \Gamma_2 P_1^{n+1} + T_2 Q_2^{n+1} \quad (31)$$

where $\Gamma_{1,2}$ and $T_{1,2}$ are reflection and transmission coefficients given by

$$\Gamma_1 = \frac{(c_2\epsilon_2 - c_1\epsilon_1)}{c_2\epsilon_2 + c_1\epsilon_1} \quad (32)$$

$$T_1 = \frac{2\epsilon_2 c_1}{c_2\epsilon_2 + c_1\epsilon_1} \quad (33)$$

$$\Gamma_2 = \frac{(c_1\epsilon_1 - c_2\epsilon_2)}{c_2\epsilon_2 + c_1\epsilon_1} \quad (34)$$

$$T_2 = \frac{2\epsilon_1 c_2}{c_2\epsilon_2 + c_1\epsilon_1} \quad (35)$$

From (30), it is clear that the right-going wave in material 2 is a sum of a transmitted portion of the right-going wave in material 1 plus a reflected portion of the left-going wave in material 2. A similar argument can be made for the left-going wave in material 1. In fact, the reflection coefficients $\Gamma_{1,2}$ can be shown to be identical to the classical Fresnel reflection coefficients. The transmission coefficients also have the same form as the Fresnel transmission coefficients. Special care needs to be taken when the LBS calculates the solution at grid points $i - 1$ and $i + 1$ for a material interface at grid point i . At grid point $i - 1$, the term Q_{i+1}^n in (23) becomes Q_1^n . At grid point i , the terms P_i^n and Q_i^n in (22) and (23) become P_1^n and Q_2^n , respectively. At grid point $i + 1$, the term P_{i-1}^n in (22) becomes P_2^n . Rearranging equations (18) and (19) for grid point i we have

$$(1 + a_1 \Delta t) P_1^{n+1} = P_{i-1}^{n-1} + (1 - 2\nu_1) (P_1^n - P_{i-1}^n) - b_1 \Delta t Q_1^n \quad (36)$$

$$(1 + a_2 \Delta t) Q_2^{n+1} = Q_{i+1}^{n-1} - (1 - 2\nu_2) (Q_{i+1}^n - Q_2^n) - b_2 \Delta t P_2^n \quad (37)$$

where $\nu_1 = c_1 \Delta t / \Delta x$, and $\nu_2 = c_2 \Delta t / \Delta x$. The terms a_1, a_2, b_1, b_2 refer to the a and b coefficients in (12) and (13) for materials 1 and 2, respectively. These equations are now easily solved for P_1^{n+1} and Q_2^{n+1} and then (30) and (31) are applied to obtain P_2^{n+1} and Q_1^{n+1} .

4 Outer Boundary Condition

The outer radiation boundary condition is used to terminate the computational lattice and permit outgoing waves to pass unreflected through the lattice boundaries [13]. The FDTD algorithm uses a spatial central difference operator where it uses field values from neighboring cells to update solution variables. Thus it cannot be used at the terminating faces of the problem domain. For example, the solution for a wave propagating left to right will eventually require a grid point outside the domain. To terminate the computational lattice, an additional equation (boundary condition) is needed to solve the system and this introduces information into the solution that is not required by Maxwell's equations.

On the contrary, the LBS requires no extraneous boundary condition. For the present LBS implementation, like the Method of Characteristics [9], the interior point algorithm calculates the left-going characteristic at the left boundary (i.e. $i = 0$) and the right-going characteristic at the right boundary (i.e. $i = imax$). Thus for the LBS, at grid point $i = 0$, equation (21) calculates $Q(0)$ and the incoming right-going characteristic, $P(0)$, is specified as a boundary condition. This same analysis applies at the right boundary where (20) calculates $P(imax)$ and the incoming left-going characteristic, $Q(imax)$, is specified as a boundary condition. Shang [14] has noted for characteristic based multidimensional and nonuniform grid problems, in principle, the local coordinate system can be rotated to align with the characteristics, and the compatibility equations provide an exact boundary condition. However, a simple, yet effective approximation for multidimensional characteristic based approaches is to set the incoming flux or characteristic variables at the outer boundaries to zero and let the interior point algorithm predict the outgoing variables. When the wave motion is aligned with a coordinate axis, this boundary condition is exact.

5 Fourier Analysis

Various excellent Fourier analyses of the LBS have already been completed [3], [2], [6], [7], [8]; therefore, only the important results and conclusions from these previous analyses will be reviewed in this report. Most of the information presented is summarized from [2]. The stability condition for the LBS is $\nu \leq 1$, where ν is the Courant number $\nu = c\Delta t/\Delta x$. The normalized phase velocity for the classical leapfrog or FDTD algorithm is given by

$$\frac{c^*}{c} = \frac{\nu \sin(k\Delta x)}{\sin(\omega\Delta t)} \quad (38)$$

Making the substitution $k\Delta x = 2\pi/N$ and $\omega\Delta t = 2\pi\nu/N$, where N is the number of points per wavelength, (38) becomes

$$\frac{c^*}{c} = \frac{\nu \sin(2\pi/N)}{\sin(2\pi\nu/N)} \quad (39)$$

The leading error term of the phase speed error is given by

$$\frac{4\pi^2}{6N^2}\nu(\nu^2 - 1) \quad (40)$$

It is clear from this error term that the FDTD algorithm is second-order accurate. For the LBS, the dispersion relation is

$$\frac{c^*}{c} = \frac{(2\nu - 1) \sin(\pi/N)}{\sin(2\pi\nu/N - \pi/N)} \quad (41)$$

The leading error term of the phase speed error for the LBS is

$$\frac{4\pi^2}{12N^2} \nu (1 - \nu) (1 - 2\nu) \quad (42)$$

Results are shown in Figure 3 for the normalized phase speeds at different Courant numbers (ν) for the FDTD method and the LBS. To achieve less than 1% phase speed error requires about $N = 15$

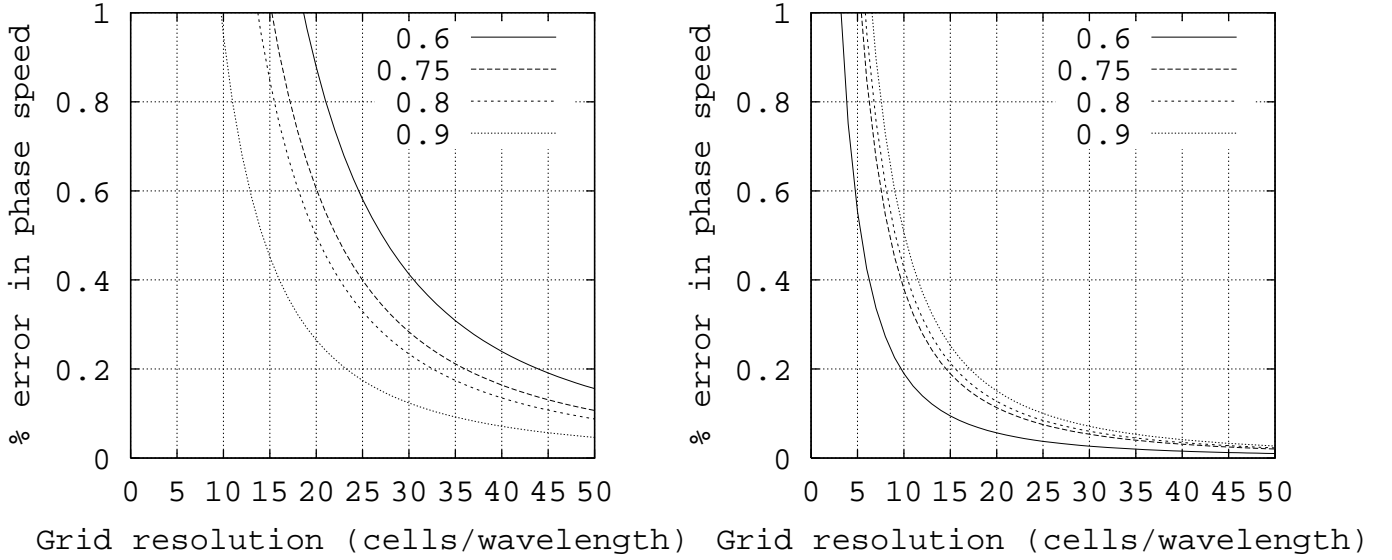


Figure 3: Percentage error in phase speed versus grid resolution for (a) the FDTD method; and (b) the LBS. Plot parameter is ν , the Courant number.

for the FDTD method and about $N = 6$ for the LBS. Note that the LBS has zero dispersion error for $\nu = 1$ and $\nu = 0.5$. Based upon these results, the LBS method is about 2-3 times as economical as the FDTD method for the same level of accuracy.

6 Results

Since the LBS has previously been applied to free-space propagation problems on uniform grids [4], [7], this report concentrates on one-dimensional model problems involving free-space propagation on nonuniform grids and reflection from lossy dielectric materials on both uniform and nonuniform grids. The problem space size is 1000 cells with nonperiodic boundary conditions. For the uniform grid, a space step size of 1 cm is used, the time step is 0.33 ps and the Courant number $\nu = 1$. For the boundary conditions, a Gaussian point source at $i = 0$ is used to

specify $P(0)$ and $Q(1000) = 0$. For many complex geometries, it is often desirable to implement nonuniform grids to reduce the computational effort and memory resources and to improve modeling accuracy. We define a nonuniform grid by using a mesh stretch ratio of $M \equiv \Delta x_{max}/\Delta x_{min}$ which is periodic every 10 cells. Figure 4 shows an expanded view of a typical one-dimensional non-uniform grid with a mesh stretch ratio of 3 and a periodicity of 10 cells. The Courant num-

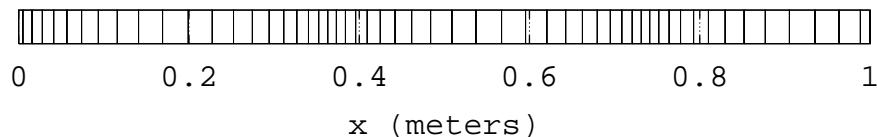


Figure 4: Section of a one-dimensional non-uniform grid with a mesh stretch ratio of 3 and a base cell size of 1 cm. The grid variation is periodic every 10 cells.

ber for a nonuniform grid is defined by $c\Delta t/\Delta x_{min}$, where Δx_{min} is the smallest cell size in the nonuniform grid.

The first problem is a free space propagation problem on a nonuniform grid with a mesh stretch ratio of 2 that is periodic every 10 cells. In this case, periodic boundary conditions are used and the Gaussian pulse is allowed to propagate for 724 meters, which leads to a time integration of 90,504 time steps. The Courant number $\nu = 0.8$, the time step was $\Delta t = 2.67$ ns and the Gaussian pulse had a FWHM pulse width of 2.26 ns. This pulse contained significant spectral content up to 1 GHz. Figure 5 shows the error in the electric field after $n = 90,504$ time steps for both the FDTD method and the LBS. Note for this particular problem, the error for the LBS is exceptionally

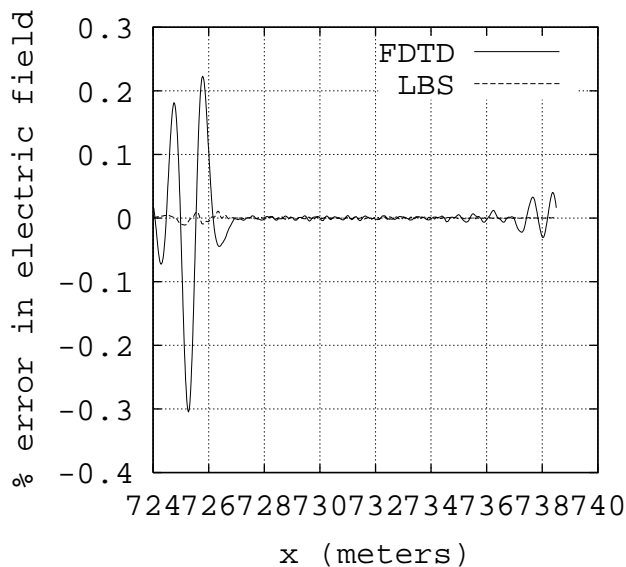


Figure 5: Percent error in electric field for a free space propagation problem on a nonuniform grid using the FDTD method and the LBS.

low. From further experimentation, it was demonstrated that the LBS provided excellent results (within 0.1% accuracy) up to a mesh stretch ratio of 3.

The next problem involved reflection and transmission for a lossy dielectric half-space. A uniform grid was used first with the dielectric half-space for $5 \leq x \leq 10$ m with material parameters $\epsilon_{r2} = 4$, $\sigma_2 = 0.02$, $\sigma_2^* = 0$ and $\mu_{r2} = 1$ and with $\nu = 1$. This problem tests the implementation of the dielectric surface boundary condition which exists in the grid at cell $i = 500$. Figure 6 shows the time-domain scattered electric field for both the LBS and the FDTD method at cell $i = 400$. Note the agreement between the two methods is almost indistinguishable. The complex

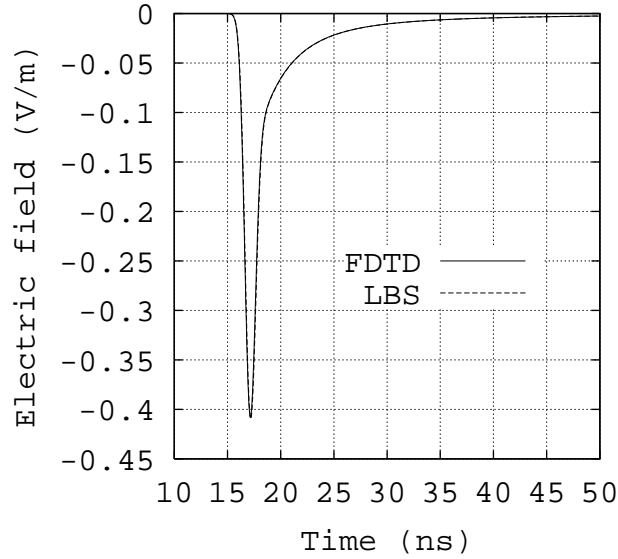


Figure 6: Time-domain electric field recorded at cell $i = 400$ for reflection from a lossy dielectric half-space using FDTD and the LBS on a uniform grid.

reflection coefficient was calculated at cell $i = 400$ for both methods and is plotted in Figure 7 along with the exact solution. The agreement between methods is again excellent. Next, a lossless dielectric was inserted in the uniform grid domain for $5 \leq x \leq 10$ m with material parameters $\epsilon_{r2} = 80$, $\sigma_2 = \sigma_2^* = 0$ and $\mu_{r2} = 1$. The complex reflection coefficient was computed from the time-domain fields and is shown in Figure 8. Clearly the LBS is superior in this instance, with a reflection coefficient that overlays the exact solution. Note that the LBS solution is exact for this case because of the exact implementation of the physical boundary conditions on the electromagnetic field for the LBS. The lossy dielectric results were not as accurate because the dielectric boundary conditions assumed a frequency-independent impedance. If the frequency dependent surface impedance were used, then the results would be more accurate. Finally, the same lossy dielectric problem was analyzed on a nonuniform grid which is periodic every 10 cells and with a mesh stretch ratio of 2. The material parameters were again $\epsilon_{r2} = 4$, $\sigma_2 = 0.02$, $\sigma_2^* = 0$ and $\mu_{r2} = 1$. The dielectric surface boundary condition remains at $i = 500$, which puts the x coordinate for the boundary at 7.24 meters. Electric field data was recorded at $x = 5$ meters (i.e. $i = 346$). The time-domain fields are shown in Figure 9 and Figure 10 shows the reflection coefficient magnitude

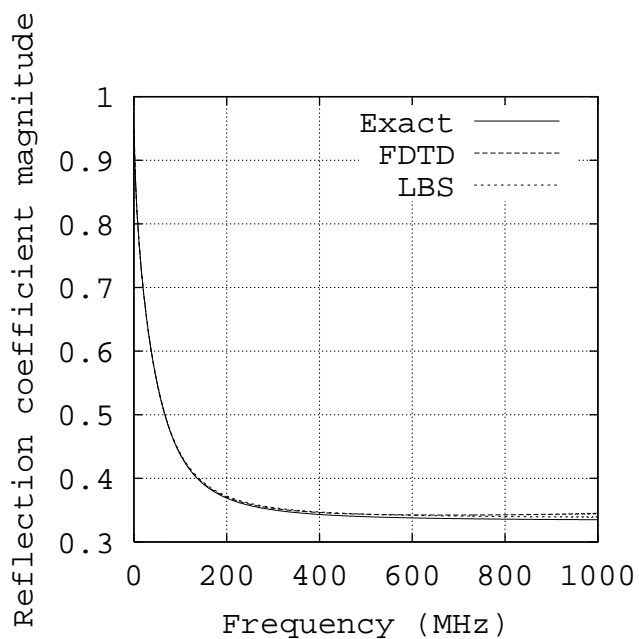


Figure 7: Reflection coefficient magnitude versus frequency for reflection from a lossy dielectric half-space using FDTD and the LBS on a uniform grid.

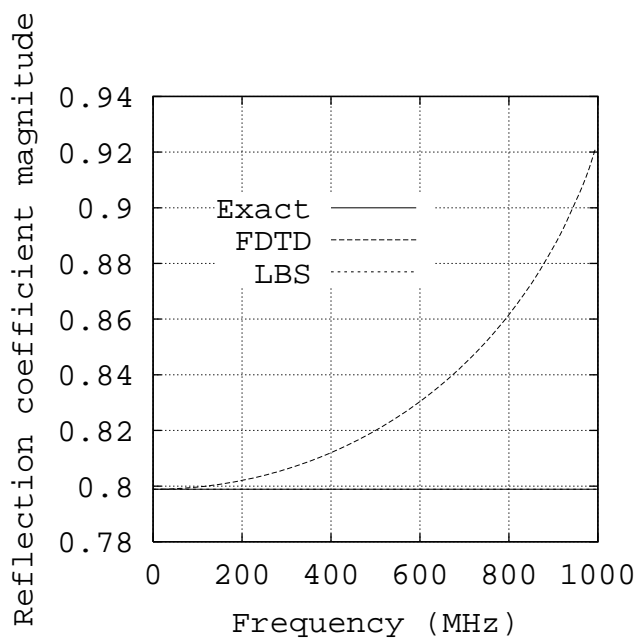


Figure 8: Reflection coefficient magnitude versus frequency for reflection from a lossless dielectric half-space using FDTD and the LBS on a uniform grid.

results. We clearly see that the LBS is superior on a nonuniform grid, with a reflection coefficient

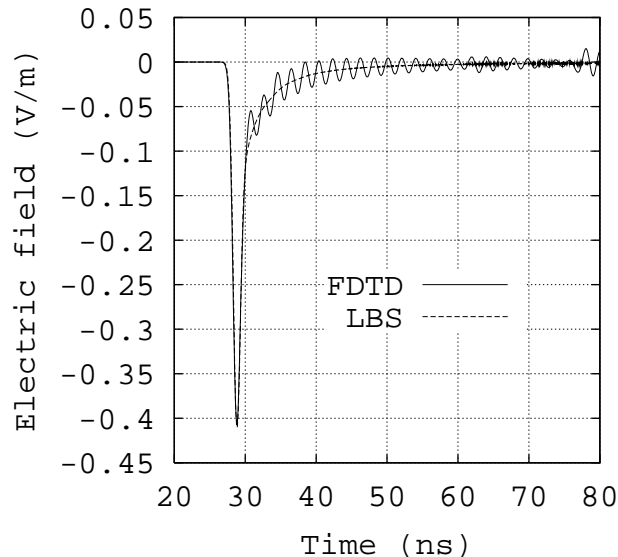


Figure 9: Time-domain electric field recorded at cell $i = 346$ for reflection from a lossy dielectric half-space using FDTD and the LBS on a non-uniform grid.

accuracy level within 2%. Further results for uniform and nonuniform grids and perfect conductors can be found in [15].

7 Conclusions

This report has extended the Linear Bicharacteristic Scheme for computational electromagnetics to model homogeneous and heterogeneous lossy dielectric and magnetic materials and perfect conductors. It was demonstrated that the LBS has several distinct advantages over conventional FDTD algorithms. First, the LBS is a second-order accurate algorithm which is about 2-3 times as economical. The LBS can also be made to have zero dispersion error in certain instances. Second, the LBS provides a more natural and flexible way to implement surface boundary conditions and outer radiation boundary conditions by using characteristics and an upwind bias technique popular in fluid dynamics. Third, the LBS provides more accurate results on nonuniform grids. The upwind biasing provides a more flexible generalization to unstructured grids. A dielectric surface boundary condition was implemented and results were provided for several one-dimensional model problems involving lossy dielectric materials and free space. The results indicate that the LBS is a superior algorithm for treatment of dielectric materials, especially its performance on nonuniform grids. Based upon these results, the LBS is a very promising alternative to a conventional FDTD algorithm for many applications. Extensions to two and three-dimensional problems should be straightforward.

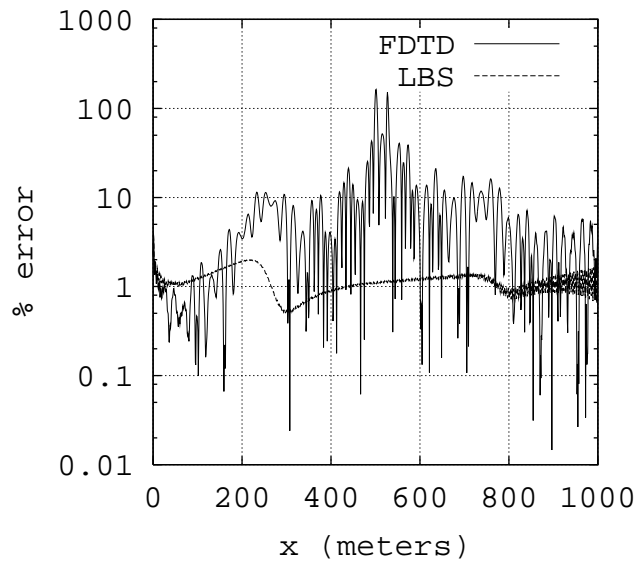


Figure 10: Percent error in reflection coefficient magnitude versus frequency for reflection from a lossy dielectric half-space using FDTD and the LBS on a non-uniform grid.

References

- [1] J. D. Hoffman, *Numerical Methods for Engineers and Scientists*, McGraw-Hill, New-York, 1992.
- [2] P. Roe, "Linear bicharacteristic schemes without dissipation," Tech. Report 94-65, ICASE, NASA/Langley Research Center, Hampton, VA, 1994.
- [3] J. P. Thomas and P. L. Roe, "Development of non-dissipative numerical schemes for computational aeroacoustics," AIAA, 1993, paper number 93-3382-CP.
- [4] B. Nguyen and P. Roe, "Application of an upwind leap-frog method for electromagnetics," in *Proc. 10th Annual Review of Progress in Applied Computational Electromagnetics*, Monterey, CA, March 1994, Applied Computational Electromagnetics Society, pp. 446–458.
- [5] J. P. Thomas, C. Kim and P. Roe, "Progress toward a new computational scheme for aeroacoustics," in *AIAA 12th Computational Fluid Dynamics Conference*. AIAA, 1995.
- [6] J. P. Thomas, *An Investigation of the Upwind Leapfrog Method for Scalar Advection and Acoustic/Aeroacoustic Wave Propagation Problems*, Ph.D. thesis, University of Michigan, Ann Arbor, MI, 1996.
- [7] B. Nguyen, *Investigation of Three-Level Finite-Difference Time-Domain Methods for Multidimensional Acoustics and Electromagnetics*, Ph.D. thesis, University of Michigan, Ann Arbor, MI, 1996.
- [8] C. Kim, *Multidimensional Upwind Leapfrog Schemes and Their Applications*, Ph.D. thesis, University of Michigan, Ann Arbor, MI, 1997.

- [9] J. H. Beggs, D. L. Marcum and S. L. Chan, "The numerical method of characteristics for electromagnetics," *Applied Computational Electromagnetics Society Journal*, vol. 14, no. 2, pp. 25-36, July 1999.
- [10] A. Iserles, "Generalized leapfrog methods," *IMA Journal of Numerical Analysis*, vol. 6, pp. 381-392, 1986.
- [11] A. Yefet and P. Petropoulos, "A non-dissipative staggered fourth-order accurate explicit finite-difference scheme for the time-domain Maxwell's equations," Tech. Report 99-30, ICASE, NASA/Langley Research Center, Hampton, VA, 1999.
- [12] A. Taflove, Ed., *Advances in Computational Electrodynamics: The Finite-Difference Time-Domain Method*, Artech House, Boston, MA, 1998.
- [13] A. Taflove, *Computational Electrodynamics: The Finite-Difference Time-Domain Method*, Artech House, Boston, MA, 1995.
- [14] J. S. Shang, "A fractional-step method for solving 3D time-domain Maxwell equations," in *AIAA 31st Aerospace Sciences Meeting & Exhibit*, Reno, NV, Jan. 1993, vol. AIAA 93-0461.
- [15] S. L. Chan, "The linear bicharacteristic scheme for electromagnetics," M.S. thesis, Mississippi State University, Starkville, MS, Dec. 1999.

